Buckling of Oval Cylindrical Shells under Compression and Asymmetric Bending

Y.N. Chen* and Joseph Kempner†
Polytechnic Institute of New York, Brooklyn, N.Y.

Bifurcation buckling of oval cylindrical shells under the interaction of uniform compressive forces and bending moments of arbitrary orientation is investigated. Buckling loads as well as the asymmetric buckling modes are determined by a matrix interative solution aided by a sequence of successive approximate solutions.

Nomenclature

$a_j, \bar{a}_j$	= Fourier coefficients of X_2 and X_3, respectively
E	= modulus of elasticity
$f(F), f^\circ(F^\circ)$	= bifurcation and prebuckling stress functions, respectively; dimensionless form in parentheses
h	= shell thickness
$I_2(J_2), I_3(J_3)$	= moments of inertia of oval cross section with respect to the axes x_2 and x_3, respectively
K	= thickness parameter denoting the quantity $[12(1-\upsilon^2)]^{1/2}(r_0/h)$
$\bar{M}(M)$	= terminal bending couple
N	= average axial force per unit circumferential length
$\bar{P}(P)$	= applied end thrust
$r(R)$	= radius of curvature of the cross-sectional contour
r_0	= average radius of the oval cross section
$s(S)$	= circumferential coordinate
$w(W)$	= inward normal displacement at the bifurcation state
$x(X)$	= axial coordinate
$x_2(X_2), x_3(X_3)$	= rectangular coordinates of the cross section
z_{ij}	= component of a matrix z containing the eigenvectors z_1, z_2, z_3, z_4
z_1, z_2, z_3, z_4	= eigenvectors
α	= nondimensional axial wave length
β	= angle formed between the moment vector and the x_3 axis
ξ	= eccentricity parameter
φ_2, φ_3	= quantities defined by Eqs. (13)
λ	= eigenvalue defined as $1/M^2$
υ	= Poisson's ratio

Introduction

THE stability of circular and noncircular cylindrical shells under uniform axial compression has been extensively studied, both experimentally and analytically. However, the problem of nonuniform compression of noncircular cylindrical shells has not received sufficient attention. Uniform loading is rarely achieved in practice, though the problem of collapse of shell structures resulting from pure bending is as important as that concerned with collapse due to uniform axial compression.

Received June 27, 1975; revision received Jan. 15, 1976. Research sponsored by the Air Force Office of Scientific Research, Air Force Systems Command, USAF, under AFOSR Contract/Grant F44620-74-C-0047.

Index categories: Structural Stability Analysis; Structural Static Analysis.

*Associate Professor of Applied Mechanics.

†Professor and Head, Department of Aerospace Engineering and Applied Mechanics. Associate Fellow AIAA.

Some historical background may be projected by the work of Flügge,[1] of Seide and Weingarten,[2] and of Abir and Nardo,[3] to cite only a few. These articles explore the linear buckling of circular cylindrical shells caused by pure bending couples applied at the ends of the cylinder. We reported earlier[4] some results of an analysis dealing with the stability of oval cylindrical shells under the combined action of uniform axial compression and bending couples. In that paper, both buckling and initial postbuckling (with imperfection sensitivity like that of Koiter-Budiansky-Hutchinson) were discussed. Most recently, Koroleva[5] published a buckling study of the same nature based on a finite-difference approach that yielded results qualitatively identical to that of Ref. 4.

It should be noted that the state of axial stress, as well as the corresponding deformation in Refs. 4 and 5, were restricted to be symmetric with respect to the major or minor axis of the oval cross section. For the sake of completeness alone, the antisymmetric modes of buckling should be taken into account. In the present work, the analysis of Ref. 4 is extended to permit an arbitrary orientation of the applied couples. To this end, both the symmetric and antisymmetric modes must be taken into the formulation. Mathematically, in addition to doubling the size of the resulting eigenvalue problem, difficulties of iterative convergence arise from the loose coupling of two linear systems whose largest eigenvalues can be extremely close. Such difficulties are resolved by a procedure of sequential approximation.

Stability Equation

In Ref. 4, the validity of the Donnell-type shell equations in the prebuckling, buckling, and initial postbuckling analysis of noncircular cylindrical shells subjected to bending by terminal couples, and to compression by uniform axial forces, was discussed at considerable length. Without repeating their development, the resulting differential equations governing the state of neutral equilibrium are adopted here.‡ The two differential equations are written here in nondimensional form as

$$\nabla^4 W - (K/R)F_{,XX} - F^\circ_{,SS} W_{,XX} = 0 \tag{1}$$

$$\nabla^4 F + (K/R)W_{,XX} = 0 \tag{2}$$

In the preceding equations, the nondimensional variables and operators are defined as follows:

$$W = w/h, \quad F = Kf/(Eh^2 r_0), \quad F^\circ = K^2 f^\circ/(Ehr_0^2),$$

$$K = [12(1-\upsilon^2)]^{1/2} r_0/h,$$

$$(\mathrm{R},\mathrm{X},\mathrm{S},\mathrm{X}_2,\mathrm{X}_3) = (\mathrm{r},\mathrm{x},\mathrm{s},\mathrm{x}_2,\mathrm{x}_3)/r_0$$

‡The length of the cylinder is assumed to be of the order of one to two times the major axis, so that general flattening of the cross section of the Brazier type is not present.

where w and f, respectively, are the inward deflection and Airy stress function developed at the bifurcation point; υ is Poisson's ratio and E is Young's modulus of elasticity; r and r_0, respectively, are the local and average radii of curvature; f° denotes the Airy stress function for the prebuckling resultant forces. A comma indicates partial differentiation with respect to the ensuing subscript, and the operator $\nabla^4(\ )$ is the two-dimensional biharmonic operator in the $X-S$ coordinate system. In particular,

$$F^\circ_{,SS} = (K^2/Eh) f^\circ_{,ss} = (K^2/Eh) \int_{-h/2}^{h/2} \sigma_x^0 dz \tag{3}$$

in which σ_x^0 represents the prebuckling axial normal stress. All other symbols appearing in the preceding definitions are shown in Fig. 1. It should be noted that the circumferential length of the oval cross section is equal to $2\pi r_0$.

If a pair of compressive forces $\bar{P}=2\pi r_0 N$ and a pair of couples $\bar{M}$ are applied to the ends of the oval cylinder, with the moment vector forming an angle β with the horizontal axis x_3, it can be shown easily that the prebuckling axial normal stress, measured by $F^\circ_{,SS}$, is given by

$$F^\circ_{,SS} = -(K^2/Eh)[N + (hx_2/I_3)\bar{M}\cos\beta + (hx_3/I_2)\bar{M}\sin\beta]$$

where I_2 and I_3 are the cross-sectional moments of inertia about the x_2 and x_3 axes, respectively. Upon the introduction of the nondimensional compressive force P, moment M, and moments of inertia J_2 and J_3, such that

$$(J_2, J_3) = (I_2, I_3)/I_0, \quad I_0 = \pi r_0^3 h,$$

$$P = NK/(2Eh), \quad M = \bar{M}Kr_0/(2EI_0)$$

the above expression becomes

$$F^\circ_{,SS} = -2K(P + MX_2\cos\beta/J_3 + MX_3\sin\beta/J_2) \tag{4}$$

The final form of the governing differential equation can now be obtained by combining Eqs. (1,2, and 4), through which the functions F and F° are eliminated, resulting in

$$\nabla^4 W + (K/R)\nabla^{-4}[(K/R)W_{,XXXX}]$$

$$+2K[P + M(X_2\cos\beta/J_3 + X_3\sin\beta/J_2)]W_{,XX} = 0 \tag{5}$$

in which ∇^{-4} is the inverse operator of ∇^4. If β and P are set equal to zero, Eq. (5) reduces to a form equivalent to the stability equations obtained in Ref. 4.

Solution of Stability Equation

The radius of curvature $R(S)$ is chosen here to be expressed as $R = 1/(1+\xi\cos 2S)$, to describe a doubly symmetric oval section. It can be shown[6] that, for such an oval section, the nondimensional rectangular coordinates X_2 and X_3 of a point on the contour curve are given by the following expansions:

$$X_2 = \sum_{j=1,3\ldots}^{\infty} a_j \cos jS, \quad X_3 = \sum_{j=1,3\ldots}^{\infty} \bar{a}_j \sin jS \tag{6}$$

The coefficients of the first five terms of the expansions, which depend upon the eccentricity parameter ξ, are given by

$$a_1 = 1 + \xi/4 - \xi^2/16 - \xi^3/128 + \xi^4/1024 + \ldots$$

$$a_3 = (\xi/12)(1 - \xi/8 - \xi^2/32 + \xi^3/384 + \ldots)$$

$$a_5 = (\xi^2/160)(1 + \xi/12 - \xi^2/48 + \ldots)$$

$$a_7 = (\xi^3/2688)(1 - \xi/16 + \ldots)$$

$$a_9 = \xi^4/55296 + \ldots$$

$$\bar{a}_i(\xi) = |a_i(-\xi)| \qquad (i = 1,3\ldots) \tag{7}$$

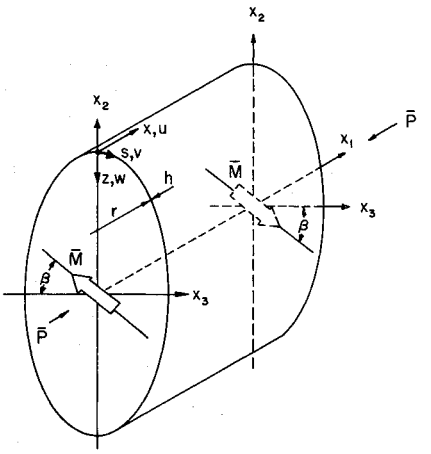

Fig. 1 Sign convention and shell geometry.

For practical purposes, the expansions given by Eqs. (6) can be truncated after a_9 and $\bar{a}_9$; i.e., $a_j = \bar{a}_j = 0$ if $j > 9$.

Since the orientation of the moment vector is arbitrary, no symmetry conditions with respect to the circumferential coordinate can be imposed. The solution to Eq. (5) is therefore assumed to be in the form

$$W = [z_{11}/\sqrt{2} + \sum_{j=2}^{\infty} z_{1j}\cos 2(j-1)S + \sum_{j=1}^{\infty} z_{3j}\cos(2j-1)S$$

$$+ \sum_{j=1}^{\infty} z_{2j}\sin 2jS + \sum_{j=1}^{\infty} z_{4j}\sin(2j-1)S]\cos(X/\alpha) \tag{8}$$

After some straightforward calculations, it can be shown that the displacement parameters z_{ij} $(i=1,2,3,4)$ must satisfy the following system of matrix equations:

$$A_1 z_1 = \lambda^{-1/2}(\varphi_3 B_1 z_3 + \varphi_2 B_2 z_4) \tag{9}$$

$$A_2 z_2 = \lambda^{-1/2}(\varphi_3 B_3 z_4 + \varphi_2 B_4 z_3) \tag{10}$$

$$A_3 z_3 = \lambda^{-1/2}(\varphi_3 B_1^T z_1 + \varphi_2 B_4^T z_2) \tag{11}$$

$$A_4 z_4 = \lambda^{-1/2}(\varphi_3 B_3^T z_2 + \varphi_2 B_2^T z_1) \tag{12}$$

In these matrix equations

$$\lambda = 1/M^2, \quad \varphi_3 = (1/J_3)\cos\beta, \quad \varphi_2 = (1/J_2)\sin\beta \tag{13}$$

The superscript T denotes the transpose of a square matrix. The symbols A_i and B_i $(i=1,2,3,4)$ denote eight square matrices whose components are given as follows:

Matrices A_i:

$$A_1(j,j) = Q_{2j-2} + 1/Q_{2j-2} + (\xi/2)^2(Q_{2j-4} + Q_{2j}) - 2P$$

$$A_1(j,j+1) = (\xi/2)(Q_{2j-2} + Q_{2j})$$

$$A_1(j,j+2) = (\xi/2)^2 Q_{2j}$$

$$A_2(j,j) = Q_{2j} + 1/Q_{2j} + (\xi/2)^2(Q_{2j-2} + Q_{2j+2}) - 2P$$

$$A_2(j,j+1) = (\xi/2)(Q_{2j} + Q_{2j+2})$$

$$A_2(j,j+2) = (\xi/2)^2 Q_{2j+2}$$

$$A_3(j,j) = A_4(j,j) = Q_{2j-1} + 1/Q_{2j-1}$$

$$+ (\xi/2)^2(Q_{2j-3} + Q_{2j+1}) - 2P$$

$$A_3(j,j+1) = A_4(j,j+1) = (\xi/2)(Q_{2j-1} + Q_{2j+1})$$

$$A_3(j,j+2) = A_4(j,j+2) = (\xi/2)^2 Q_{2j+1} \tag{14}$$

where $Q_j = K\alpha^2/(1+j^2\alpha^2)^2$, in which α is a nondimensional axial wave length.

The preceding expressions are valid for $j \geq 1$ with the exception of the following terms.

$$A_1(1,1) = Q_0 + Q_0^{-1} + 2(\xi/2)^2 Q_2 - 2P$$

$$A_1(1,2) = \sqrt{2}(\xi/2)(Q_0 + Q_2)$$

$$A_1(1,3) = \sqrt{2}(\xi/2)^2 Q_2$$

$$A_1(2,2) = Q_2 + Q_2^{-1} + (\xi/2)^2(2Q_o + Q_4) - 2P$$

$$A_2(1,1) = Q_2 + Q_2^{-1} + (\xi/2)^2 Q_4 - 2P$$

$$A_3(1,1) = Q_1 + Q_1^{-1} + 2(\xi/2)Q_1 + (\xi/2)^2(Q_1 + Q_3) - 2P$$

$$A_3(1,2) = (\xi/2)(Q_1 + Q_3) + (\xi/2)^2 Q_1$$

$$A_4(1,1) = Q_1 + Q_1^{-1} - 2(\xi/2)Q_1 + (\xi/2)^2(Q_1 + Q_3) - 2P$$

$$A_4(1,2) = (\xi/2)(Q_1 + Q_3) - (\xi/2)^2 Q_1 \qquad (15)$$

Moreover, the matrices A_i are symmetric; i.e., $A_i(m,n) = A_i(n,m)$. All other terms are equal to zero.

Matrices B_i:

$$B_1(1,k) = \sqrt{2}a_{2k-1}$$

$$B_1(j,k) = (a_{2j-2k-1} + a_{2k-2j+1}) + a_{2j+2k-3} \qquad (j \geq 2,\ k \geq 1)$$

$$B_2(1,k) = \sqrt{2}\bar{a}_{2k-1}$$

$$B_2(j,k) = (\bar{a}_{2k-2j+1} - \bar{a}_{2j-2k-1}) + \bar{a}_{2j+2k-3} \qquad (j \geq 2,\ k \geq 1)$$

$$B_3(j,k) = (a_{2j-2k+1} + a_{2k-2j-1}) - a_{2j+2k-1} \qquad (j,k \geq 1)$$

$$B_4(j,k) = (\bar{a}_{2j-2k+1} - \bar{a}_{2k-2j-1}) + \bar{a}_{2j+2k-1} \qquad (j,k \geq 1) \qquad (16)$$

Evidently, the size of the system of equations given by Eqs. (9-12) can be reduced by one half, by eliminating z_3 and z_4 by means of Eqs. (11) and (12). The reduction leads to a simpler system of equations

$$C_{11}z_1 + C_{12}z_2 = \lambda z_1$$

$$C_{21}z_1 + C_{22}z_2 = \lambda z_2 \qquad (17)$$

in which

$$C_{11} = A_1^{-1}[\varphi_3^2 B_1 A_3^{-1} B_1^T + \varphi_2^2 B_2 A_4^{-1} B_2^T]$$

$$C_{12} = A_1^{-1}[\varphi_2\varphi_3(B_1 A_3^{-1} B_4^T + B_2 A_4^{-1} B_3^T)]$$

$$C_{21} = A_2^{-1}[\varphi_2\varphi_3(B_3 A_4^{-1} B_2^T + B_4 A_3^{-1} B_1^T)]$$

$$C_{22} = A_2^{-1}[\varphi_3^2 B_3 A_4^{-1} B_3^T + \varphi_2^2 B_4 A_3^{-1} B_4^T] \qquad (18)$$

and A_i^{-1} denotes the inverse of A_i.

Successive Approximations

Equations (17) can be solved by a simple iterative procedure, by substituting the vectors z_1 and z_2 obtained from the right-hand side into the left-hand side of the equations. In most cases, fast convergence toward the mode of the highest eigenvalue can be expected, which leads to the determination of the largest eigenvalue λ and the associated eigenvectors z_1 and z_2. Nevertheless, when applied to the present class of problems, the convergence is prohibitively slow, if good starting vectors z_1 and z_2 are not available, because the two highest eigenvalues are, at times, very close.[7] In fact, with the added arithmetic errors induced in the computation, the process may even diverge.

However, if good starting vectors can be constructed, as is the case in the ensuing discussion, such a simple iterative procedure can readily yield the desired results.

First, let the matrices C_{12} and C_{21} be ignored, to pose a group of two eigenvalue problems uncoupled to each other, in which the deformations are symmetric and antisymmetric, respectively, with respect to the major axis of the oval cross section

$$C_{11}z_1^* - \lambda_1^* z_1^* = 0 \qquad C_{22}z_2^* - \lambda_2^* z_2^* = 0 \qquad (18)$$

which can be iteratively solved with ease. Let this formulation be designated as Problem 1.

Next, let

$$z_1 = \mu_1 z_1^* + \mu_3 z_2^*, \quad z_2 = \mu_2 z_2^* + \mu_4 z_1^* \qquad (19)$$

where z_1^* and z_2^* are solutions to Problem 1, corresponding to the largest eigenvalues λ_1^* and λ_2^*, respectively. A functional U can be constructed such that

$$U = \tfrac{1}{2}z_1^T A_1(C_{11}z_1 + C_{12}z_2 - \lambda z_1) + \tfrac{1}{2}z_2^T A_2(C_{21}z_1 + C_{22}z_2 - \lambda z_2)$$

It should be noted that if the components of z_1 and z_2 are independently varied, the condition of minimizing U with respect to these independent parameters leads to Eqs. (17). Upon minimizing U with respect to μ_i $(i=1,2,3,4)$, the following eigenvalue problem is posed by a matrix equation of the form

$$D\mu = \lambda G\mu \qquad (20)$$

where $\mu = \{\mu_i\}$, and D and G are two symmetric (4×4) matrices. This problem is designated as Problem 2.

Finally, by setting $\mu_3 = \mu_4 = 0$ in Problem 2, it follows that

$$\begin{bmatrix} z_1^{*T}A_1C_{11}z_1^* & z_1^{*T}A_1C_{12}z_2^* \\ z_1^{*T}A_2C_{21}z_2^* & z_2^{*T}A_2C_{22}z_2^* \end{bmatrix}\begin{bmatrix}\mu_1\\ \mu_2\end{bmatrix} = \lambda^{**}\begin{bmatrix} z_1^{*T}A_1z_1^* & 0 \\ 0 & z_2^{*T}A_2z_2^* \end{bmatrix}\begin{bmatrix}\mu_1\\ \mu_2\end{bmatrix}$$

and by virtue of Eqs. (18), it follows that

$$\begin{bmatrix} k_1(\lambda_1^* - \lambda^{**}) & k_2 \\ k_2 & k_3(\lambda_2^* - \lambda^{**}) \end{bmatrix}\begin{bmatrix}\mu_1\\ \mu_2\end{bmatrix} = 0$$

where

$$k_1 = z_1^{*T}A_1z_1^*, \quad k_2 = z_1^{*T}A_1C_{12}z_2^*, \quad k_3 = z_2^{*T}A_2z_2^*$$

Here $k_1 \geq 0$, and $k_3 \geq 0$, since A_1 and A_2 are positive definite. The eigenvalues are obtained as

$$\lambda^{**} = \tfrac{1}{2}\{\lambda_1^* + \lambda_2^* \pm [(\lambda_1^* - \lambda_2^*)^2 + k_2^2/k_1k_3]^{1/2}\} \qquad (21)$$

Clearly, $\lambda^{**} \geq \max(\lambda_1^*, \lambda_2^*)$. If the upper sign in Eq. (21) is chosen, the associated eigenvector components μ_1^{**} and μ_2^{**} can be easily determined. This is designated as Problem 3.

The procedure of the successive approximation scheme now emerges. The approximate eigenvectors z_1 and z_2 are constructed by solving Problems 1, 3, and 2 in sequence. These vectors are then utilized as the first approximation needed for the iterative solution of Eqs. (17).

Engineering Approximation

In Ref. 4, an engineering approximation was suggested for the interaction problem corresponding to the one discussed in

the present report, with $\beta=0°$ or $\beta=90°$. This simplified estimation of the interacting loads was based on the criterion that the cylindrical shell's critical state is reached whenever the prebuckling axial compression normal stress equals the classical value of $\sigma_{cr}=2E/(KR)$. Here, $R=R(S)$ denotes the local value of the nondimensional radius of curvature. It is now suggested that such an approximation can be readily extended to the present interaction problem, in which the orientation of the applied moments is arbitrary.

If the ratio of the prebuckling axial normal stress, to the aforementioned classical stress, is set equal to unity, it follows that $R[P+M(X_2\varphi_3+X_3\varphi_2)]=1$. Thus, the interaction curve may be obtained from either

$$M_{cr}=\underset{0\le S\le\pi/2}{\text{MIN}}\ [(1/R-P)/(X_2\varphi_3+X_3\varphi_2)] \quad (22)$$

for given values of P, or

$$P_{cr}=\underset{0\le S\le\pi/2}{\text{MIN}}\ [(1/R)-M(X_2\varphi_3+X_3\varphi_2)] \quad (23)$$

The minimization with respect to S, after which the "buckling point" $S=S^*$ is also determined, can be carried out numerically without difficulty.

Discussion of Results

The numerical computation follows the procedure outlined in the section "Successive Approximations." In all cases, the axial compressive force $P(P\ge 0)$ is maintained as constant, while the axial wavelength parameter α is determined so as to yield the smallest possible value of the bending moment M.

Evidently, the four vectors z_1, z_2, z_3, and z_4 couple through Eqs. (9-12), and the collection of these four vectors forms the eigenvector. The degenerate cases of $\beta=0°$ and $\beta=90°$ present a somewhat different situation. For instance, when $\beta=0°$ ($\varphi_2=0$), z_1 and z_3 contribute to the mode of deformation symmetric with respect to the major axis of the oval cross section, while z_2 and z_4 form the antisymmetric mode. On the other hand, when $\beta=90°$ ($\varphi_3=0$), z_1 and z_4 represent the parameters of the mode symmetric with respect to the minor axis, while z_2 and z_3 belong to the antisymmetric counterpart. Thus, in all cases, symmetry is spoken of with reference to the plane of the applied moments.

First, the cases of pure bending were computed by setting $P=0$. Results corresponding to the symmetric modes were found to be identical to those obtained in Ref. 4. However, for a large portion of the two curves $\beta=0°$ and $\beta=90°$ in Fig. 2, the antisymmetric mode yields buckling moments that are slightly lower than those of the symmetric mode. For instance, for $\xi=0$ (circular cylinder), the nondimensional moment corresponding to the symmetric mode and the antisymmetric mode are found to be 1.03 and 1.00, respectively, and are associated with two distinct values of α, each of which minimizes the corresponding buckling moment. While these revised curves do not differ substantially from the curves of the symmetric modes, they reveal the situation that causes the difficulties encountered in the coupled problems of $0°<\beta<90°$.

For example, with $\beta=2°$, $\xi=0.5$, $\alpha=0.03055$, buckling moments of the symmetric and the antisymmetric mode of Problem 1, in which the coupling is ignored, are found to be 1.6072 and 1.6095, respectively. Subsequently, Problem 3 results in $M=M_1=1.5974$ and $M=M_2=1.6193$. These densely packed roots are, indeed, very close to the first and second roots of the complete eigenvalue problem posed by Eqs. (17), which indicates weak coupling of the symmetric and antisymmetric modes. In fact, in this example, the final buckling moment is $M=1.5669$. A situation such as this (Ref. 7 for example) requires a great deal of effort to achieve iterative convergence. In actual computation, iteration simply failed to converge. Fortunately, with the procedure of sequential approximation outlined previously, convergence is accomplished, requiring far less computing time than in the exact and complete solution of the eigenvalue problem by any accessible package known to the authors.

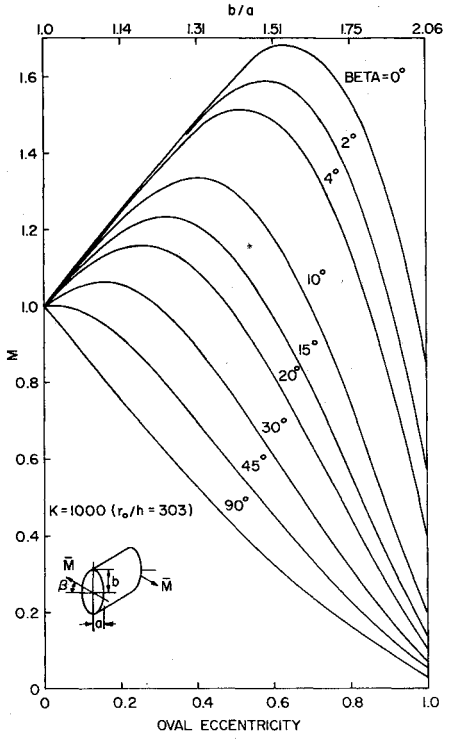

Fig. 2 Nondimensional buckling moment with orientation angle β vs. oval eccentricity parameter ξ.

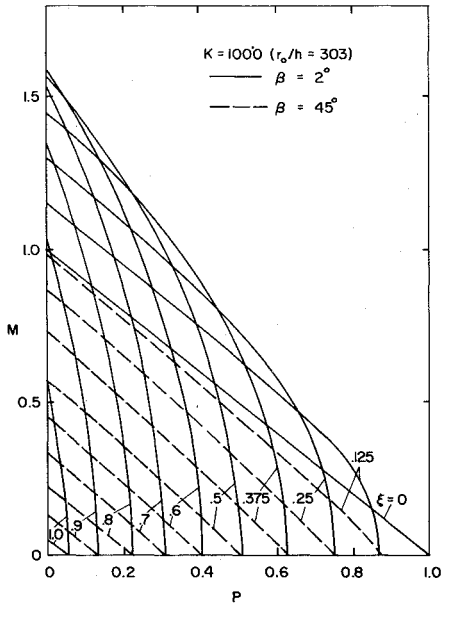

Fig. 3 Interaction curves of oval cylinders for various values of eccentricity parameter ξ and orientation angle β.

The family of buckling curves of pure bending in the range of $0°\le\beta\le 90°$ is presented in Fig. 2. The tendency of most of the curves to cluster above the lowest buckling curve ($\beta=90°$) is evident. However, when β is less than 45°, at least for oval cylinders with small to moderate eccentricity, buckling moments higher than or close to that of the circular cylinder ($\xi=0$) in the family are still possible.

For $P\ge 0$, results were obtained corresponding to β equal to 2°, 15°, 30°, and 45°. Only the results for $\beta=2°$ and 45° are

Table 1 Interaction data: axial compression vs bending moment for various values of eccentricity parameter ξ and orientation angle β ($r_0/h = 303$, $\nu = 0.3$)

ξ	P	M			
		$\beta = 2^\circ$	15°	30°	45°
0.125	0.0	1.1523	1.1293	1.061	0.9761
	0.15	0.9984	0.9740	0.9185	0.8198
	0.30	0.8444	0.8139	0.7388	0.6616
	0.45	0.6901	0.6512	0.5722	0.5011
	0.60	0.5349	0.4785	0.3976	0.3364
	0.75	0.3589	0.2759	0.2056	0.1639
	0.85	0.1634	0.0880	0.0539	0.0398
0.25	0.0	1.3001	1.2181	1.0314	0.8732
	0.12	1.1742	1.0754	0.8889	0.7425
	0.24	1.0478	0.9267	0.7423	0.6102
	0.36	0.9186	0.7670	0.5900	0.4757
	0.48	0.7694	0.5892	0.4300	0.3384
	0.60	0.5769	0.3843	0.2286	0.1968
	0.72	0.2643	0.1176	0.0677	0.0490
0.375	0.0	1.4489	1.2234	0.9212	0.7315
	0.1	1.3383	1.0801	0.7905	0.6210
	0.2	1.2141	0.9224	0.6565	0.5094
	0.3	1.0699	0.7568	0.5182	0.3964
	0.4	0.8942	0.5735	0.3745	0.2817
	0.5	0.6677	0.3655	0.2236	0.1647
	0.6	0.3136	0.1133	0.0624	0.0447
0.5	0.0	1.5669	1.1216	0.7586	0.5766
	0.075	1.4547	0.9901	0.6557	0.4947
	0.150	1.3225	0.8520	0.5509	0.4125
	0.225	1.1776	0.7059	0.4439	0.3295
	0.300	1.0052	0.5496	0.3344	0.2457
	0.375	0.7943	0.3796	0.2218	0.1611
	0.450	0.5097	0.1900	0.1051	0.0754
0.6	0.0	1.5873	0.9719	0.6111	0.4532
	0.05	1.4871	0.8739	0.5417	0.4001
	0.10	1.3757	0.7726	0.4715	0.3467
	0.15	1.2575	0.6677	0.4005	0.2930
	0.20	1.1219	0.5583	0.3286	0.2392
	0.25	0.9728	0.4439	0.2556	0.1850
	0.30	0.7946	0.3231	0.1814	0.1305
	0.35	0.5725	0.1943	0.1059	0.0757
0.7	0.0	1.5281	0.7783	0.4603	0.3354
	0.05	1.3802	0.6712	0.3913	0.2840
	0.10	1.2365	0.5604	0.3215	0.2325
	0.15	1.0691	0.4453	0.2510	0.1806
	0.20	0.8743	0.3250	0.1795	0.1286
	0.25	0.6341	0.1984	0.1071	0.0763
0.8	0.0	1.3419	0.5589	0.3145	0.2263
	0.04	1.1988	0.4681	0.2605	0.1869
	0.08	1.0394	0.3749	0.2059	0.1474
	0.12	0.8571	0.2787	0.1510	0.1077
	0.16	0.6386	0.1790	0.0956	0.0680
	0.20	0.3480	0.0755	0.0396	0.0281
0.9	0.0	1.0318	0.3339	0.1808	0.1290
	0.025	0.9080	0.2755	0.1481	0.1055
	0.050	0.7710	0.2161	0.1153	0.0820
	0.075	0.6149	0.1555	0.0823	0.0585
	0.100	0.4286	0.0937	0.0492	0.0349
	0.125	0.1787	0.0305	0.0159	0.0112
1.0	0.0	0.5725	0.1378	0.0727	0.0516
	0.012	0.4854	0.1097	0.0577	0.0409
	0.024	0.3890	0.0814	0.0426	0.0302
	0.036	0.2289	0.0527	0.0275	0.0195
	0.048	0.1454	0.0238	0.0124	0.0087

displayed in Fig. 3, with the oval eccentricity ξ as a parameter. The remaining data, as well as those plotted in Fig. 3, are tabulated in Table 1. In Fig. 3, the curves seem to form two distinct groups. The solid curves ($\beta = 2^\circ$) appear to be highly nonlinear and resemble those of the so-called "strong oval," classified in Ref. 4 and herein corresponding to $\beta = 0^\circ$. On the other hand, the almost linear dashed lines ($\beta = 45^\circ$) identify with the interaction curves of the so-called "weak oval," corresponding to $\beta = 90^\circ$. For a given value of ξ, the two sets of curves, as well as those which lie in between, merge, as expected, at the abscissa on which $M = 0$. With the data summarized in Table 1, the intermediate curves can be filled in the wedge-like area bounded by the dashed curves from below, and by the solid curves from above. This is exemplified by the typical plot for $\xi = 0.6$ in Fig. 4. In this figure, the transition from the strong-type ($\beta = 0^\circ$) to the weak-type ($\beta = 90^\circ$) of interaction is illustrated. As in the case of pure bending, the curves also cluster above the curve of $\beta = 90^\circ$. Thus, the orientation of the bending couples plays an important role in the stability of oval cylinders when bending couples are present. This point is well demonstrated in the two cross plots in Figs. 5 and 6. In Fig. 5, the axial force P is plotted against β for constant values of the moment M, while in Fig. 6, M is plotted

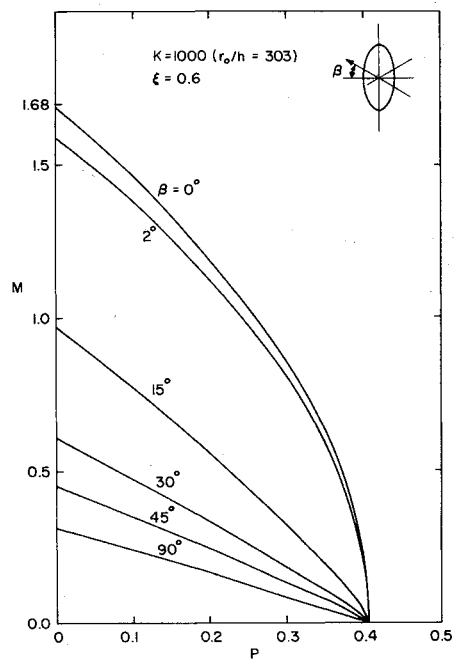

Fig. 4 Interaction curves of an oval cylinder ($K = 1000$, $\xi = 0.6$) for various values of β.

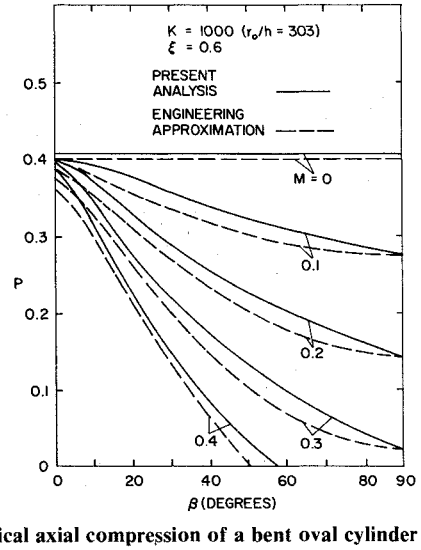

Fig. 5 Critical axial compression of a bent oval cylinder for various values of the moment orientation angle.

against β for constant values of P. In both cases the critical load decreases rapidly as β increases from 0° to 90°. Although Figs. 4-6 are based on results corresponding to $\xi = 0.6$, the qualitative picture is generally the same for all oval cylinders considered in the present work.

Some typical buckling patterns are displayed in Fig. 7. Of interest is the fact that the buckling patterns shown in this figure are virtually antisymmetric with respect to the major axis ($S = 0$). Among the computed cases this skew pattern occurs much more often than does the symmetric one. Moreover, the locations of the buckling points, indicated by the highest peaks of the curves, demonstrate the tendency of favoring the ends of the minor axis, $(s/2\pi r_0) = 0.25$ (the least rigid region), rather than the point where the maximum compressive stress occurs; this tendency is even greater for larger values of β. This observation bears out the earlier contention that eccentrically loaded oval cylinders are more likely to collapse in the weak mode (Figs. 2-6), a marked departure from the behavior of a circular cylinder under similar loading conditions.

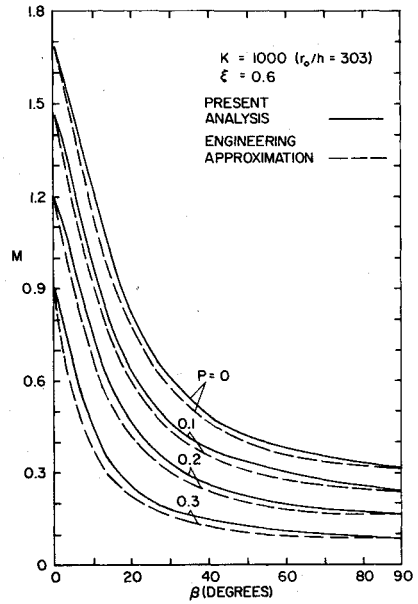

Fig. 6 Bifurcation moment of an axially compressed oval cylinder vs. the orientation angle.

Finally, the engineering estimates of the interacting loads were computed according to Eqs. (22) and (23). Comparison between such results with the analytical results presented in Table 1, as well as with those shown in Figs. 2-6 (the solid lines) is favorable, with the approximate results being somewhat below those of the exact solution. The discrepancy is believed to be primarily a result of the dependency of the actual buckling load on the thickness, and is similar to that observed in Ref. 4 for $P=0$, $\beta=0°$, and 90°. Some of the results based on the engineering approximation are presented in Figs. 5 and 6 as dashed lines. Although only limited comparison is shown, it should be noted that such favorable comparison is typical for all cases computed.

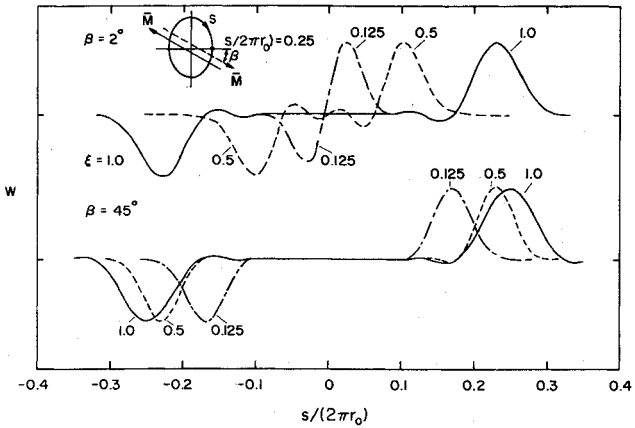

Fig. 7 Buckling patterns of an oval cylinder subjected to bending.

References

[1] Flügge, W., "Die Stabilitat der Kreiszylinderschale," *Ingenieur-Archiv*, Vol. 3, 1932, pp. 463-506.

[2] Seide, P. and Weingarten, V.I., "On the Buckling of Circular Cylindrical Shells under Pure Bending," *Journal of Applied Mechanics,* Vol. 28, March 1961, pp. 112-116.

[3] Abir, D. and Nardo, S.V., "Thermal Buckling of Circular Cylindrical Shells under Circumferential Temperature Gradients," *Journal of the Aerospace Sciences,* Vol. 26, Dec. 1959, pp. 803-808.

[4] Kempner, J. and Chen, Y.N., "Buckling and Initial Postbuckling of Oval Cylindrical Shells under Combined Axial Compression and Bending," *Transactions of the New York Academy of Sciences,* Series 11, Vol. 36, No. 2, 1974, pp. 171-191.

[5] Koroleva, E.M., "Stability of Cylindrical Shells of Oval Cross-Section in the Bending State of Stress," *Prikladnaya Matematika i Mekhanika*, Vol. 37, June 1974, pp. 901-903.

[6] Romano, F.J. and Kempner, J., "Stress and Displacement Analysis of a Simply-Supported Noncircular Cylindrical Shell under Lateral Pressure, *Journal of Applied Mechanics,* Vol. 29, Dec. 1962, pp. 669-674.

[7] Faddeev, D.K. and Faddeeva, V.N., *Computational Methods of Linear Algebra*, W.H. Freeman and Co., San Francisco, 1963, pp. 179-225.